# From Layered Molybdic Acid to Lower-Dimensional Nanostructures by Intercalation of Amines under Ambient Conditions

Mohammed Ibrahim Shukoor,[†] Helen Annal Therese,[†] Lela Gorgishvili,[†] Gunnar Glasser,[‡] Ute Kolb,[§] and Wolfgang Tremel*[,†]

*Institut für Anorganische Chemie und Analytische Chemie, Johannes Gutenberg-Universität, Duesbergweg 10-14, D-55099 Mainz, Germany, Max Planck-Institut für Polymerforschung, Ackermannweg 10, D-55128 Mainz, Germany, and Institut für Physikalische Chemie, Johannes Gutenberg-Universität, Welderweg 11, D-55099 Mainz, Germany*

*Received July 29, 2005. Revised Manuscript Received January 26, 2006*

Nanostructures of varied dimensionality such as rods, scrolls, and disks of molybdenum oxide have been synthesized in gram quantities under ambient conditions using exfoliation of the layers as a synthetic tool. Intercalation of alkylamines ($C_nH_{2n+2}NH_2$, where $n = 3$, 4, 8, 12, and 16) into yellow molybdic acid ($MoO_3 \cdot 2H_2O$) and subsequent treatment with nitric acid resulted in molybdenum oxide nanorods, nanodisks, or oxide−amine composite nanorods. The sizes of the nanoparticles range from a few nanometers to micrometers in length and 10 to 200 nm in diameter. Detailed X-ray, scanning electron microscopy, and transmission electron microscopy analyses reveal an inverse relation between the size of the nanoparticles and the chain length of the guest molecules. Infrared and thermogravimetric studies throw light on the driving force for the amine intercalation and the orientation of the intercalated amine molecules.

## Introduction

Moving to lower dimensionality has always been innovative and resulted in diverse applications. Anisotropic nanoparticles such as nanorods, nanotubes, nanowires, nanobelts, and nanocrystals are more important as they provide model systems for property studies based on dimension, direction, and size.[1−3] The large surface area exposed by nanomaterials facilitates the surface functionalization with organic molecules. This may lead to ordered hierarchical arrangements of organic−inorganic composites and opens a broad area of nanoscopically structured functional materials.[4−6] One important way to synthesize low-dimensional nanomaterials is to use a layered precursor. Conversion of inorganic layered materials to nanosheets by exfoliation has attracted keen interest because nanosheets can be used as a component for novel supramolecular assemblies applicable in nanoscience and nanotechnology.[7]

One of the most important advantages of layered materials is their ability to intercalate organic guest molecules into their interlayer spaces, thereby resulting in exfoliation of sheets and turning them into one-dimensional (1D) form. Various materials composed of a wide variety of compositions and structures have been synthesized using exfoliated nanosheets which can be cast or spin-coated onto substrates to form thin films.[8] A layer-by-layer assembly has been utilized for the formation of more complex nanosystems using suspensions of inorganic layered materials.[9] Polymer−clay nanocomposites are a typical example of the use of exfoliated clay minerals.[10] Moving back to the history of exfoliation, layered materials such as titanates, niobates, phosphates, and so forth have been successfully exfoliated. Nanosheets of $Nb_6O_{17}$ bilayers were obtained by the intercalation of alkylamines under hydrothermal treatment from $K_4Nb_6O_{17}$ crystals.[11] Saupe et al. were successful in exfoliating the layers of potassium hexaniobate with tetra(*n*-butyl) ammonium hydroxide ($TBA^+OH^-$) to form nanoscale tubules[12] whereas Du et al. used alkylamines along with $TBA^+OH^-$.[13] Layered titanates were exfoliated under ambient conditions using $TBA^+OH^-$ [14] and also were intercalated with alkyldiamines.[15] Taking advantage of layered metal

* To whom correspondence should be addressed. Fax: (+49) 6131-39-25605. Tel.: (+49) 6131-39-25135. E-mail: tremel@mail.uni-mainz.de.
[†] Institut für Anorganische Chemie und Analytische Chemie, Johannes Gutenberg-Universität.
[‡] Max Planck-Institut für Polymerforschung.
[§] Institut für Physikalische Chemie, Johannes Gutenberg-Universität.

(1) Patzke, G. R.; Krumeich, F.; Nesper, R. *Angew. Chem., Int. Ed.* **2002**, *41*, 2446.
(2) Tenne, R. *Angew. Chem., Int. Ed.* **2003**, *42*, 5124.
(3) Rao, C. N. R.; Nath, M. *Dalton Trans.* **2003**, 1.
(4) Torimoto, T.; Maeda, K.; Maenaka, J.; Yoneyama, H. *J. Phys. Chem.* **1994**, *98*, 13658.
(5) O'Regan, B.; Grätzel, M. *Nature* **1991**, *353*, 737.
(6) (a) Tahir, M. N.; Eberhardt, M.; Therese, H. A.; Kolb, U.; Theato, P.; Mueller, W. E. G.; Schröder, H.-C.; Tremel, W. *Angew. Chem., Int. Ed.* **2006**, *45*, 908. (b) Therese, H. A.; Rocker, F.; Reiber, A.; Li, J.; Stepputat, M.; Glasser, G.; Kolb, U.; Tremel, W. *Angew. Chem., Int. Ed.* **2005**, *44*, 262.
(7) Kaschak, D. M.; Lean, J. T.; Waraksa, C. C.; Saupe, G. B.; Usami, H.; Mallouk, T. E. *J. Am. Chem. Soc.* **1999**, *121*, 3435.
(8) Abe, R.; Shinohara, K.; Tanaka, A.; Hara, M.; Kondo, J. N.; Domen, K. *Chem. Mater.* **1998**, *10*, 329.
(9) Keller, S. W.; Kim, H. N.; Mallouk, T. E. *J. Am. Chem. Soc.* **1994**, *116*, 8817.
(10) Lan, T.; Kaviratna, P. D.; Pinnavaia, T. J. *Chem. Mater.* **1995**, *7*, 2144.
(11) Miyamoto, N.; Yamamoto, H.; Kaito, R.; Kuroda, K. *J. Chem. Soc., Chem. Commun.* **2002**, 2378.
(12) Saupe, G. B.; Waraksa, C. C.; Kim, H.-N.; Han, Y. J.; Kaschak, D. M.; Skinner, D. M.; Mallouk, T. E. *Chem. Mater.* **2000**, *12*, 1556.
(13) Du, G.; Chen, Q.; Yu, Y.; Zhang, S.; Zhou, W.; Peng, L.-M. *J. Mater. Chem.* **2004**, *14* (9), 1437.
(14) Sasaki, T.; Watanabe, M. *J. Am. Chem. Soc.* **1998**, *120* (19), 4682.

10.1021/cm051685a CCC: $33.50 
Published on Web 03/28/2006

phosphate exfoliation work was carried out on α-hafnium, α-tin, and vanadium phosphates using *n*-alkylamines[16−18] and with $TBA^+OH^-$ in zirconium phosphate.[19] Moving to more complicated systems such as perovskite tungstates, exfoliation was carried out using quarternary ammonium hydroxides leading to nanoscale colloids.[20] Transition metal oxides and chalcogenides such as $TiO_2$, $V_2O_5$, $MoO_3$, $MoS_2$, and $WS_2$ are only a few to name from the layered wealth, which have been extensively studied because of their applications as discussed.[1]

The synthesis of organic−inorganic nanocomposites by intercalation of amines into layered inorganic materials has been known for some time. Amines are excellent guest molecules, which can easily be intercalated into the interlayer spaces of inorganic materials by displacing the sodium or potassium cations, protons, or the water molecules residing between the layers of the two-dimensional (2D) inorganic compounds. Recently Chandrappa et al.[21] have synthesized macroporous $V_2O_5$−amine composites in a single step reaction by intercalation of hexadecylamine (HDA) into layered $V_2O_5$ in the presence of hydrogen peroxide by utilizing the exothermic reaction between amines and $H_2O_2$. In general, the intercalation of organic guest molecules requires elevated temperatures, and in most cases intercalation was carried out hydrothermally.[22−25]

Molybdenum oxide and its derivatives are widely used in industry as catalysts, display devices, sensors, smart windows, or battery electrodes.[26−30] Syntheses of $MoO_3$ rods and tubes using solvothermal,[31] hydrothermal,[22,32,33] and thermal decomposition[34] techniques were reported; however, the above-mentioned techniques need high-temperature or (super)critical conditions.

In this article we present a simple technique for the synthesis of $MoO_3$ nanorods, disks, and scrolls using layered yellow molybdic acid and amines as starting materials under ambient conditions. The intercalation mechanism of amines with different alkyl chain lengths and the role of different amines on the morphology of the $MoO_3$ nanoparticles are also discussed.

## Experimental Section

$MoO_3 \cdot 2H_2O$ (yellow) was synthesized as reported by Freedman[35] followed by intercalation of amines of varying chain lengths, namely, propyl-, butyl-, octyl-, dodecyl-, and hexadecylamine. In a typical experiment, a mixture of 10 mM of yellow molybdic acid and 5 mM of amine along with 20 mL of a solution containing ethanol and water in a 1:3 ratio was stirred for approximately 48 h, until a white solid powder was obtained. Subsequently, the molybdenum oxide−amine composite was stirred with 33% $HNO_3$ for two more days at room temperature. The final product was then washed with water and dried. In the case of HDA intercalation the molybdenum oxide−propylamine (PA) composite was used as the starting material. To gain a deeper insight into the reaction kinetics, a detailed study was carried out using IR and X-ray powder diffraction (XRD) analysis on octylamine (OA) intercalated yellow molybdic acid composites prepared with reaction times of 6, 12, 18, 24, and 48 h.

**Characterization.** The products were characterized using scanning electron microscopy (SEM; LEO 1530 field-emission scanning electron microscope, 6 kV extraction voltage) and transmission electron microscopy (TEM) using a Philips 420 instrument with an acceleration voltage of 120 kV and a Philips FEI TECNAI F30 ST electron microscope (field-emission gun, 300 kV extraction voltage). In addition, infrared spectroscopy (Mattson Instruments 2030 Galaxy FT-IR spectrometer), XRD (Seifert XRD 3000 TT diffractometer and Bruker D8 powder diffractometer, Cu Kα radiation), and thermogravimetric analysis (TGA) studies in air (NETZSCH, model STA 429) were also carried out to understand the interaction between the inorganic host and the organic guest molecules. The molybdenum content of the composites was determined using a microprobe analyzer (JEOL, JXA 8900, Analyser Crystal PET at 10 kV voltage and 5 nA current).

## Results and Discussion

Molybdenum oxide nanostructures with various morphologies were obtained using a novel route at ambient conditions. Yellow molybdic acid ($MoO_3 \cdot 2H_2O$) has a monoclinic crystal structure ($P2_1/n$) with cell dimensions of $a = 10.476$ Å, $b = 13.833$ Å, $c = 10.606$ Å, and $\beta = 91.63°$. It adopts a layered structure where the distorted layers are constructed by corner sharing $MoO_5(H_2O)$ octahedra.[36−38] The layers are stacked along the *b* axis and interconnected by interlayer water molecules. By replacing the interlayer water molecules under mild conditions with organic templates such as primary amines of various chain lengths $C_nH_{2n+1}NH_2$ (where $n = 3$, 4, 8, 12, and 16) a control over the morphology can be gained. In a previous study, Krumeich et al.[22] have studied the intercalation of HDA into $MoO_3$ under hydrothermal conditions. Although the hydrothermal reaction yielded nanocrystals with well-defined morphologies, the reaction kinetics were not studied because of the technical complica-

(15) Airlodi, C.; Nunes, L. M.; de Farias, R. F. *Mater. Res. Bull.* **2000**, *35*, 2081.
(16) Rodriguez, M. L.; Surez, M.; Garcia, J. R.; Rodriguez, J. *Solid State Ionics* **1993**, *63−65*, 488.
(17) Takenaka, A.; Ozeki, Y.; Hiraki, S.; Hattori, M.; Motooka, I.; Nariai, H. J. *Mater. Sci.* **1996**, *31*, 6511.
(18) Dasgupta, S.; Agarwal, M.; Datta, A. *J. Mater. Chem.* **2002**, *12*, 162.
(19) Kaschak, D. M.; Johnson, S. A.; Hooks, D. E.; Kim, H.-N.; Ward, M. D.; Mallouk, T. E. *J. Am. Chem. Soc.* **1998**, *120*, 10887.
(20) Schaak, R. E.; Mallouk, T. E. *J. Chem. Soc., Chem. Commun.* **2002**, 706.
(21) Chandrappa, G. T.; Steunou, N.; Livage, J. *Nature* **2002**, *416*, 702.
(22) Niederberger, M.; Krumeich, F.; Muhr, H.-J.; Müller, M.; Nesper, R. *J. Mater. Chem.* **2001**, *11*, 1941.
(23) Wei, X. M.; Zeng, H. C. *Chem. Mater.* **2003**, *15*, 433.
(24) Xu, Y. *Chem. Mater.* **1988**, *8*, 814.
(25) Zapf, P. J.; Haushalter, R. C.; Zubieta, J. *Chem. Mater.* **1997**, *9*, 2019.
(26) Fournier, M.; Aouissi, A.; Rocchiccioli-Deltcheff, C. *J. Chem. Soc., Chem. Commun*. **1994**, (3), 307.
(27) Takenaka, S.; Tanaka, T.; Funabiki, T.; Yoshida, S. *J. Phys. Chem. B* **1998**, *102*, 2960.
(28) Tagaya, H.; Ara, K.; Kadokawa, J. I.; Karasu, M.; Chiba, K. *J. Mater. Chem.* **1994**, *4*, 551.
(29) Yang, Y. A.; Cao, Y. W.; Loo, B. H.; Yao, J. N. *J. Phys. Chem. B* **1998**, *102*, 9392.
(30) Oyama, S. T.; Zhang, W. *J. Am. Chem. Soc.* **1996**, *118*, 7173.
(31) Patzke, G. R.; Michailovski, A.; Krumeich, F.; Nesper, R.; Grunwaldt, J.-D.; Baiker, A. *Chem. Mater.* **2004**, *16*, 1126.
(32) Lou, X. W.; Zeng, H. C. *Chem. Mater.* **2002**, *14*, 4781.
(33) Tian, Y.; He, Y.; Zhu, Y. *Mater. Chem. Phys.* **2004**, *87* (1), 87.
(34) Therese, H. A.; Zink, N.; Kolb, U.; Tremel, W. *Solid State Sci.* **2006**, in press.
(35) Freedman, M. L. *J. Am. Chem. Soc.* **1959**, *81*, 3834.
(36) Günter, J. R. *J. Solid State Chem.* **1972**, *5*, 354.
(37) Boudjada, N.; Rodriguez-Carvajal, J.; Anne, M.; Figlarz, M. *J. Solid State Chem.* **1993**, *105*, 211.
(38) Krebs, B. *Acta Crystallogr., Sect. B* **1972**, *28*, 2222.

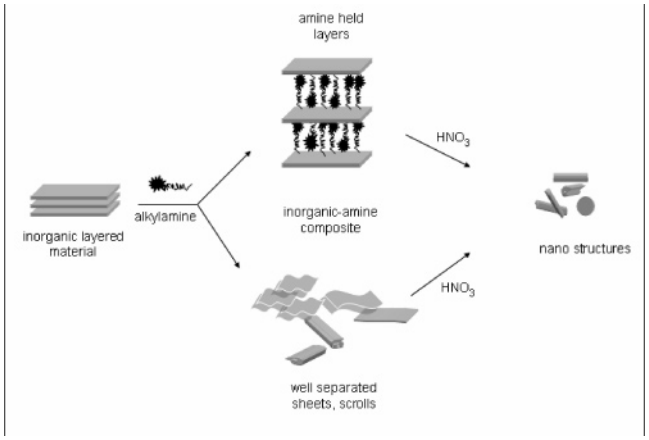


**Figure 1.** Schematic representation of amine intercalation in the layered compound.

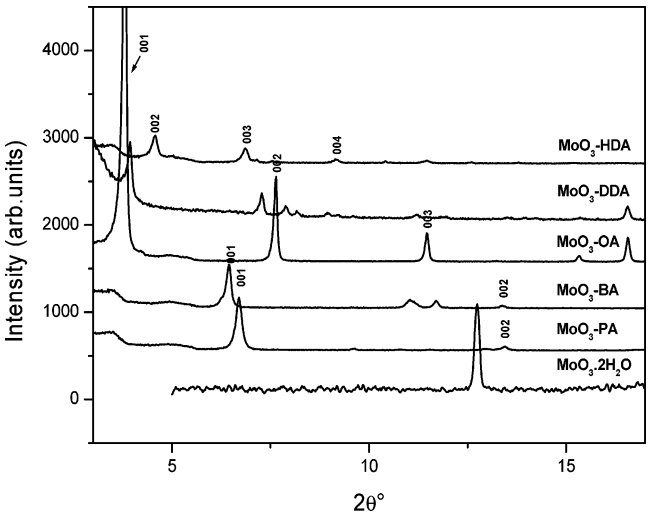


**Figure 2.** XRD patterns of $MoO_3 \cdot 2H_2O$ and various $MoO_3$−amine composites.

tions imposed by the hydrothermal conditions. To fill this gap, we have carried out a systematic study of the intercalation of various primary alkylamines into layered molybdic acid. All experiments were carried out under ambient conditions where the reaction kinetics can be monitored and an understanding of the intercalation reaction may be achieved. A summary of the synthetic approach is given in Figure 1. The starting point of the synthetic protocol is the parent layered structure ($MoO_3 \cdot 2H_2O$). Subsequently, guest molecules such as alkylamines are intercalated between the layers. The intercalation of amines should be depending strongly on the solution pH. The experiments reported in this paper were carried out at weakly basic pH, which is dictated by the p*K* values of the respective amines. Amine intercalation leads to an increase in interlayer space until the amines are comfortably accommodated. The so-formed lamellar molybdenum oxide−amine composite was treated with acid to remove amines from the interlayer space; this results in the formation of discotic and 1D nanostructures.

Yellow molybdic acid was stirred continuously with amines of various alkyl chain lengths in an ethanol/water mixture at room temperature until the yellow color of the molybdic acid changed to white. In Figure 2 the XRD patterns of the $MoO_3$−amine composites $MoO_3$−PA, $MoO_3$−butylamine ($MoO_3$−BA), $MoO_3$−OA, $MoO_3$−dodecylamine ($MoO_3$−DDA), and $MoO_3$−HDA are compared with that of the parent material ($MoO_3 \cdot 2H_2O$). The presence of alkylamines in the interlayer region of the composites can clearly be seen from the XRD patterns which exhibit sharp intense reflections at lower angles compared to yellow molybdic acid (JCPDF 39-0363), and a gradual increase in the *d* spacing of the (001) reflection is observed depending on the alkyl chain length. Molybdenum oxide composites show the 001 reflection at 12.98, 13.43, 23.2, 22.19, and 37.8 Å for $MoO_3$−PA, $MoO_3$−BA, $MoO_3$−OA, $MoO_3$−DDA, and $MoO_3$−HDA, respectively. As the alkyl chain length increases the intercalation of amines into the interlayer region of $MoO_3 \cdot 2H_2O$ becomes more difficult. Intercalation of DDA into yellow molybdic acid at room temperature resulted in a mixed phase indicating incomplete intercalation. The incomplete intercalation can be observed by the smaller *d* spacing of $MoO_3$−DDA compared to that of $MoO_3$−OA in Figure 2. This result demonstrates the difficulty in intercalating longer-chain amines at room temperature in a single reaction step. The problem could be circumvented by using $MoO_3$−PA as the starting material for HDA intercalation.

The PA intercalation increases the interlayer distance, thereby acting like a "door opener" within the starting compound, paving a path for HDA to intercalate between the layers. By means of this strategy, single-phase $MoO_3$−HDA could be obtained. The "door opening" process was explored further using an aromatic amine with a rigid organic ring. Naphthylamine was intercalated into $MoO_3$ with and without prior intercalation of PA. A comparison of the XRD data of both compounds revealed that the presence of PA accelerated the intercalation of naphthylamine into the interlayer region of molybdic acid, whereas a different material was obtained upon the intercalation of naphthylamine only (see Figure 1, Supporting Information). Further investigations showed that the products obtained vary depending on the ratio of amine to molybdenum oxide. Changing the ratio from 1:2 (as used in this study) to 1:1 for the intercalation of naphthylamine into $MoO_3$ led to significantly different results (see Figure 2, Supporting Information). A detailed study of this concentration dependent study will be the subject of a forthcoming contribution.

The morphologies of the intermediate oxide−amine intercalates were studied by SEM and TEM to understand the mechanism of the intercalation with respect to amine chain lengths. In Figure 3 we present SEM and TEM images of the amine−oxide intercalates. The images show a gradual decrease in the size of the lamellar sheets with the concomitant increase in the length of the intercalant molecules. The SEM image of $MoO_3$−PA samples in Figure 3a,b shows particles varying in size from approximately 100−500 nm. Each particle is composed of multiple lamellar sheets. The TEM image shown in Figure 3b reveals the structure of one individual particle, composed of three flakes of sheets. The SEM micrograph of the $MoO_3$−BA composite (Figure 3c) shows the presence of evenly sized particles of much smaller size (50−100 nm) compared to $MoO_3$−PA in Figure 3a. TEM analysis reveals the presence of rods or scrolls (in the inset of Figure 3d we present the image of one such sheet

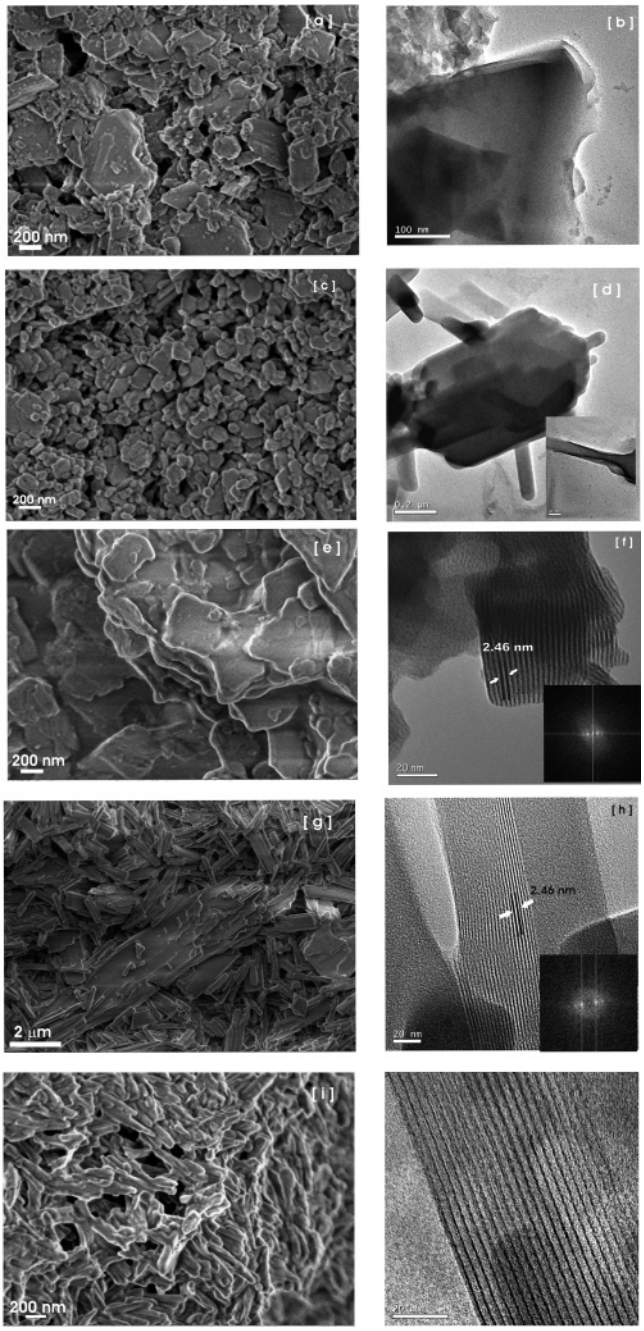


**Figure 3.** SEM and HRTEM images of $MoO_3$−PA (a, b), $MoO_3$−BA (c, d), $MoO_3$−OA (e, f), $MoO_3$−DDA (g, h), and $MoO_3$−HDA (i, j) composites, respectively. Fourier transforms are given as insets for $MoO_3$−OA and $MoO_3$−DDA in parts f and h.

which starts to roll up into a scroll) of uniform morphology along with sheetlike motifs. A selected-area electron diffraction study of the rods shows their amorphous nature, whereas the layered materials $MoO_3$−OA, $MoO_3$−DDA, and $MoO_3$−HDA have a much higher crystallinity. This becomes apparent from the high-resolution TEM (HRTEM) images in Figure 3f,h,j as well as from the Fourier transforms in Figure 3f,h. The interlayer spacings of 2.46 and 2.46 nm are in reasonable agreement with the data obtained for the bulk samples from XRD. Similarly, composites of OA intercalation (Figure 3e) depict well-separated compact particles in the size range from 50 nm to a few micrometers. Each particle contains very well-ordered sheets of OA in the interlayer region (Figure 3f). This finding is in line with

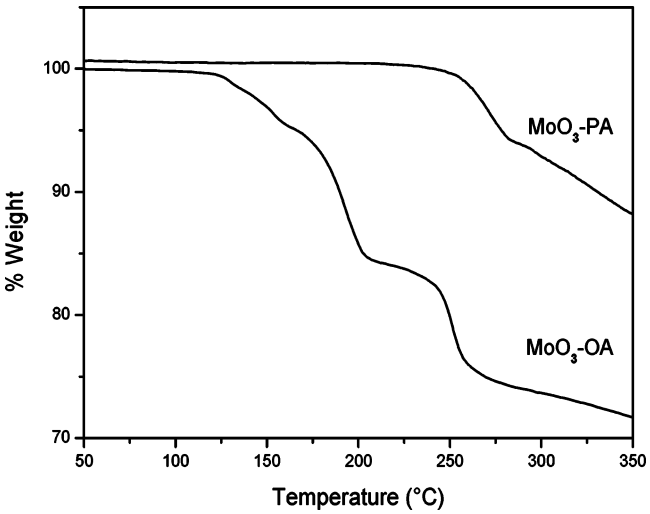


**Figure 4.** TGA traces of $MoO_3$−OA and $MoO_3$−PA under air.

the high intensity of the reflections and the long-range ordering observed for $MoO_3$−OA compared to the other oxide−amine composites in Figure 1. With increasing length of the alkyl chains the intercalation of the amines into the interlayer region becomes incomplete resulting in the formation of mixed phases. Mixtures of rods and flakes could be observed for $MoO_3$−DDA (Figure 3g) as a result of the incomplete intercalation gleaned from the TEM image in Figure 3h.

Incomplete intercalation of amines with $n > 8$ can be circumvented by using molybdic acid "pre-intercalated" with short-chain amines ($n < 8$) as the starting material. For example, the long-chain amine HDA could not be intercalated directly at ambient conditions. The SEM image of the HDA−oxide composite in Figure 3i shows a homogeneous sample consisting of short rods, which are in their initial stage of formation. The rods are 300−400 nm in length and <50 nm in diameter. In Figure 3j we present a TEM image of a HDA−oxide composite rod. The rod has a diameter of ∼60 nm and contains a stacking of 19−20 oxide layers. The large interlayer spacing indicates the presence of amines between the sheets.

Infrared spectroscopic studies show absorption bands at 2679 $cm^{-1}$, characteristic of $CH_2$ streching vibrations for all amine intercalated samples. Bands corresponding to $-NH_2$ scissoring/$NH_3^+$ bending are observed in the range of 1580−1630 $cm^{-1}$ along with broad vibrational bands in the range 2430−2790 $cm^{-1}$ typical for $NH_3^+$ symmetrical stretching. In Figure 4 we show the TGA traces of $MoO_3$−PA and $MoO_3$−OA as representatives for intercalates with short- and long-chain amines. For both samples, $MoO_3$−PA and $MoO_3$−BA, we observed a weight loss above 250 °C, which is attributed to the decomposition of intercalated amine. On the other hand, $MoO_3$−OA and $MoO_3$−HDA show a weight loss in two steps below 150 °C, which may be due to the stepwise loss of two types of water molecules. The weight loss above 150 °C could be due to the decomposition of intercalated amine in all cases. Slight differences in the decomposition temperatures may be the result of different stabilities or reactivities of intercalants with different chain lengths.

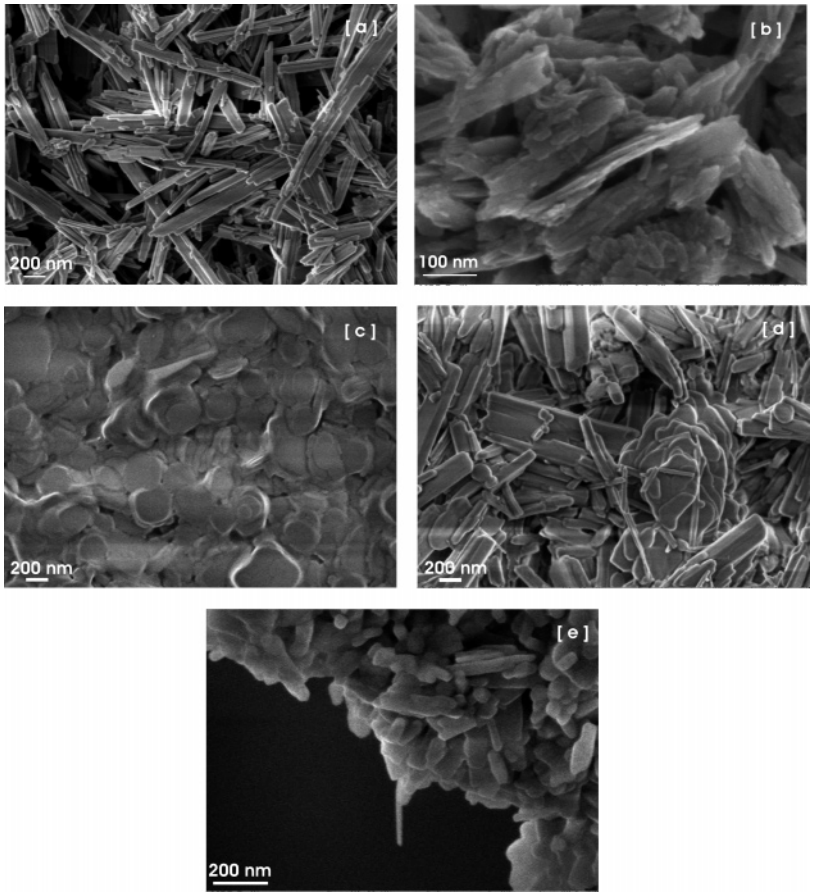


**Figure 5.** SEM images of $MoO_3$ nanostructures obtained after acid treatment of (a) $MoO_3$−PA, (b) $MoO_3$−BA, (c) $MoO_3$−OA, (d) $MoO_3$−DDA, and (e) $MoO_3$−HDA composites.

Elemental analyses combined with microprobe analyses of the composites indicate $MoO_3$/amine ratios of approximately 2:1 for $MoO_3$−PA, $MoO_3$−BA, and $MoO_3$−OA samples which are in accordance with the molar ratios of the reactants for intercalation reactions. For the mixed phases $MoO_3$−DDA and $MoO_3$−HDA, it is difficult to give reliable composition estimates.

Figure 5shows SEM pictures of the acid treated product having rodlike morphology with size specifications depending upon the length of the template molecule. $MoO_3$ oxide rods obtained using PA as the template have an average length and diameter of a few micrometers and 50−200 nm, respectively. A closer look at the micrograph in Figure 5a reveals flat, blunt-ended bundles of $MoO_3$ rods with mixed dimensions. Acid treatment of $MoO_3$−BA resulted in a mixture of products from fibrous textured sharp-ended rods to scrolls (Figure 5b). The SEM image shows agglomerated bundles of the fibers unlike the products derived from $MoO_3$−PA. HRTEM disclosed also some noncrystalline tubelike morphologies with discrete layers (see Figure 3, Supporting Information). One can clearly observe the folding of $MoO_3$ sheets resulting in a tubelike structure. Acid treatment of $MoO_3$−OA resulted in the formation of "nanodisks" (Figure 5c), and a mixed product was formed for the direct DDA intercalation into molybdic acid (Figure 5d) whereas short nanorods were formed for $MoO_3$−HDA (Figure 5e), which were pre-intercalated with PA.

**Driving Force for the Amine Intercalation.** In this study amines were intercalated at room temperature between the sheets of distorted corner-sharing $MoO_5(H_2O)$ octahedra. The driving force behind the intercalation could be related to two factors: (i) the transfer of protons from the acidic surface OH groups to the amine groups resulting in the protonation of the amines[39] or (ii) attractive electrostatic forces which assist in the intercalation of positively charged protonated amines (due to solvation) between the negatively charged inorganic layers. As the basicity or proton affinity of amines[40] is directly proportional to the chain length of the amines, the probability for the protonation of the $NH_2$ groups due to solvation also increases for amines with larger "*n*" values. Hence, the first factor (transfer of protons) for shorter-chain amines and the second factor (electrostatic attraction) for the longer-chain amines might play the major role in amine intercalation. This is also supported by the TGA results, where the presence of water is observed only in $MoO_3$−OA and $MoO_3$−HDA. These findings indicate that inclusion of water molecules goes along with the intercalation of long-chain amines. Nevertheless, irrespective of the specific driving force, $NH_3^+$ ions are expected to be present in all composites. The presence of broad vibrational bands in the IR spectra for all intercalated samples in the region 2430−2790 $cm^{-1}$, typical for $NH_3^+$ symmetric stretching,[41] is compatible with the presence of amines in their protonated

(39) Lagaly, G. *Solid State Ionics* **1986**, *22*, 43.
(40) Aue, D. H.; Webb, H. M.; Bowers, M. T. *J. Am. Chem. Soc.* **1972**, *94*, 4276.
(41) Ingham, B.; Chong, S. V.; Tallon, J. L. *J. Phys. Chem. B* **2005**, *109*, 4936 and references therein.

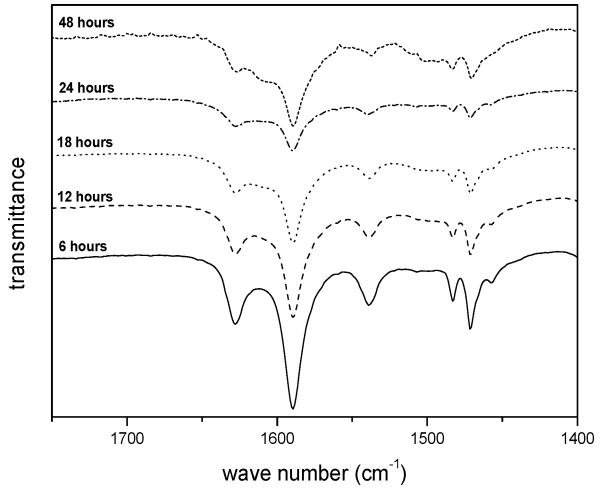


**Figure 6.** Infrared spectra of $MoO_3-OA$ composites prepared at different reaction times of 6, 12, 18, 24, and 48 h, respectively.

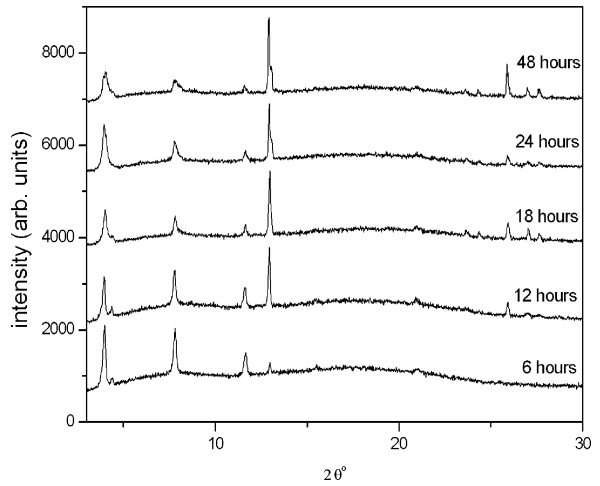


**Figure 7.** XRD patterns for the intercalation of OA into $MoO_3$ taken after reaction times of 6, 12, 18, 24, and 48 h.

forms. Figure 6 shows IR spectra of $MoO_3-OA$ composites after different reaction times. A closer look reveals bending vibration bands of OH and NH at 1590 and 1627 $cm^{-1}$, respectively.

The intensity of the bands decreases with time indicating an interaction between the amine group of the template and the oxygen of the molybdic acid, resulting in complete intercalation of amines into the $MoO_3$ interlayer spacing. This picture is supported by results from XRD shown in Figure 7. XRD data were recorded for the intercalation of OA into $MoO_3$ at intervals of 6 h. The powder pattern after 6 h shows strong low angle 00*l* reflections, which indicate a regular stacking of the $MoO_3$ layers. The intensity of the lower angle reflection decreases with time while the intensity of several reflections at larger Bragg angles increases. We attribute this observation to an ordering of the guest molecules between the layers of the host compound.

**Orientation of the Amines between the Layers.** The *d* spacings from XRD data (Figure 2) helped us to understand the mode of intercalation of the guest molecules, their orientation, and the tilting angles with respect to the host oxide layers. By plotting the interlayer spacing against the number of carbon atoms in the alkyl chain, structural information concerning the composites can be obtained

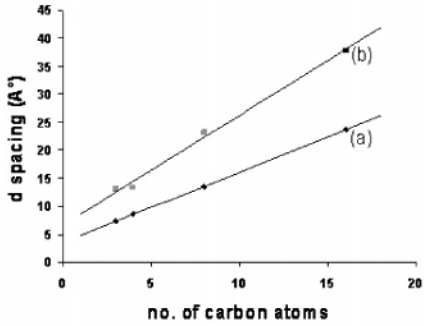


**Figure 8.** Theoretical (a) and experimental (b) plot of interlayer spacing versus number of carbon atoms in the *n*-alkyl chain of the amines.

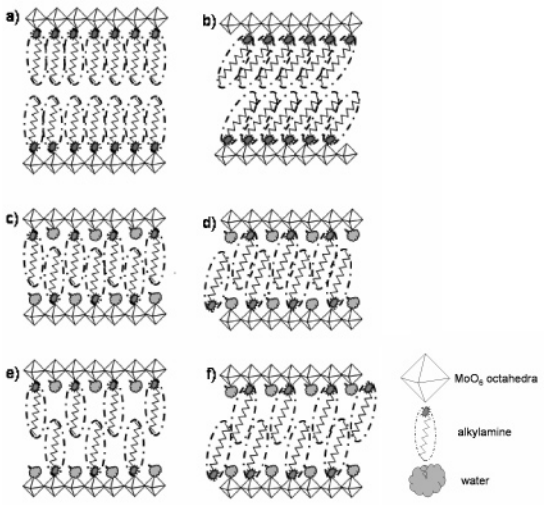


**Figure 9.** Possible orientation of guest molecules between the layers of the host lattice: (a) perpendicular non-interdigitated, (b) perpendicular, fully interdigitated, (c) perpendicular, partially interdigitated, (d) tilted, non-interdigitated, (d) tilted, fully interdigitated, and (f) tilted, partially interdigitated.

(Figure 8). As can be gleaned from the plot in Figure 8, a slope of 1.967 $Å/CH_2$ is found for the intercalates; a hypothetical slope of 1.27 $Å/CH_2$ corresponds to a single layer nontilted system. Therefore, we assume to have a bilayer system with tilted or interdigitated alkyl chains.

For the structure and orientation of the guest several models can be envisaged which are represented in Figure 9.[42] Figure 9a,c,e shows a bilayer arrangement of the guest molecules in an orientation perpendicular to the oxide layers, whereas Figure 9a shows a non-interdigitated, Figure 9c shows a fully interdigitated, and Figure 9e shows a partially interdigitated arrangement. Figure 9b,d,f shows the analogous arrangement of the guest molecules but with a tilting angle $\theta$. The non-interdigitated arrangement illustrated in Figure 9a can be ruled out as the calculated interlayer spacing is much larger than the experimental one, whereas the arrangements based on the fully interdigitated structures shown in Figure 9c,d can also be ruled out because their interlayer spacings are smaller than the experimental one. One is now left with the models illustrated in Figures 9b (non-interdigitated, tilted) and 9e,f (partially interdigitated, not tilted or tilted).

In general, the van der Waals attraction between the alkyl chains is maximized by tilting; therefore, one can also exclude the orientation shown in Figure 9e, thereby narrowing the choice to the tilted non-interdigitated and partially

**Table 1. Summary of Interlayer Spacings and Particle Morphologies for Amine Intercalates**

| | | morphology | |
|---|---|---|---|
| sample | $d_L$ (*d* spacing) | amine intercalated | acid treated |
| $MoO_3$−PA | 12.988 Å | hexagonal lamellar sheets | rods of 50−200 nm diameter and a few micrometers in length |
| $MoO_3$−BA | 13.43 Å | mixture of sheets and scrolls | rods and scrolls <60 nm in diameter and of length around 1 $\mu$m |
| $MoO_3$−OA | 23.2 Å | sheets of oxide−amine composite | disks, platelets of sizes 100−250 nm along with low percentage of rods |
| $MoO_3$−DDA | 22.19 Å | mixture of rods and sheets | rods and sheets of various sizes |
| $MoO_3$−HDA | 37.8 Å | nanorods of oxide−amine composite | rods of length 200 nm and <60 nm in diameter |

interdigitated arrangements. TGA shows the presence of water for intercalates containing long-chained amines. As the water molecules are unlikely to reside in the hydrophobic region of the non-interdigitated structure shown in Figure 9b, one can assume that the orientation of the long-chained amines follow the mode shown in Figure 9f. In contrast, the composites containing short-chain amines may prefer the non-interdigitated tilted orientation (Figure 9b).

From the slope of the plot in Figure 8 the tilting angles for the alkyl chains can be calculated. Assuming a non-interdigitated structure for the short-chain systems containg no water we can extract tilting angles of 26.33 and 20° for PA and BA. These angles are in accordance with the observed trend for the orientation of alkyl chains.[43−45] As the chain length and van der Waals interaction increase, the chains gradually move from tilted angles to a perpendicular orientation.[46−50] Because there are two free variables (tilt angle and degree of interdigitation) but only one experimental parameter (layer separation), no detailed structural model can be given.

**Particle Size Variation.** A survey of the changes in the morphology of intercalated $MoO_3$ as a function of the chain length of the guest molecules is presented in Table 1 and illustrated in Figure 10. One can see clearly from the table that the particle shapes of the composites change from 2D thick sheets to platelets to nanorods with increasing chain length "*n*" of the guest molecules $C_nH_{2n+1}NH_2$. This change in shape could be due to the breaking of sheets (during amine intercalation a separation of sheets of the molybdic acid precursor takes place) into smaller fragments as a result of large surface energy. TEM analyses also show that particles with an aspect ratio beyond a critical value have a tendency to break into smaller pieces (see Figure 3, Supporting Information). Upon acid treatment $MoO_3$−PA and $MoO_3$−BA form long and thick rods or scrolls which could result from the fast rolling of the multiple lamellae along certain specific crystal directions upon removal of the amines from the interlayer region. On the other hand, longer-chain amines remain between the oxide layer, hence retaining the morphology of the composite particles. This anomaly could be either due (i) to the low mobility of the long-chain amines, (ii) to stronger van der Waals interaction between the long alkyl chains of the amines, or (iii) to stronger interaction between the oxide layers and amines resulting from the changes in basicity.

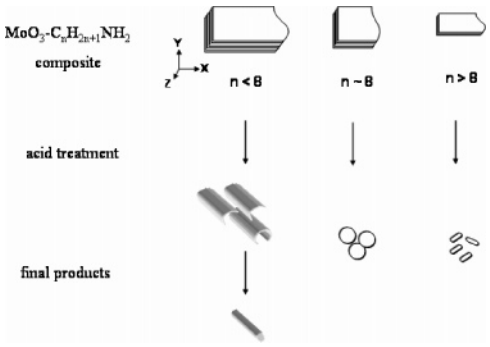


**Figure 10.** Summary of particle morphologies resulting from oxide−amine composites.

## Summary and Conclusion

We have intercalated various alkylamines into layered molybdic acid under ambient conditions, where a systematic trend in the morphologies of the composite particles is observed depending on the chain length of the guest molecules. Short-chain amines $C_nH_{2n+1}NH_2$ ($n < 9$) can easily be intercalated, while long-chain amines require a previous intercalation of short-chain amines as "door openers". The intercalation of short-chain amines proceeds by a full replacement of interlayer water molecules, while the interdigitating structure of long-chain guest molecules allows a small percentage of water molecules to remain in the voids of the interlayer space. Upon acid treatment, the short-chain amines PA and BA are removed from the interlayer region, hence resulting in an exfoliation of the oxide sheets which start rolling up because of their high surface energy forming scrolls or rods, whereas OA, DDA, and HDA remain in the interlamellar space thereby preventing any curling of the oxide layers due to enhanced interlayer interaction, which leads to a higher mechanical stability of the product composite particles and their 2D and 1D morphologies. For intermediate chain length ($n \approx 8$) the fragmentation of 2D platelets leads to the formation of compact "nanodisks". Assuming a non-interdigitated structure for the short-chain systems containing no water the tilting angles of 26.33° (PA) and 20° (BA) were calculated. Information concerning the structure and orientation of long-chain systems containing co-intercalated water guest molecules may be accessible from high-temperature X-ray studies.

In conclusion, (i) the observed product morphologies provide a working model for the morphological changes of molybdenum oxide nanocrystals. (ii) The formation of molybdenum oxide nanotubes may be envisaged from the

(42) Jacobson, A. J. In *Intercalation Chemistry*; Whittingham, M. S., Jacobson, A. J., Eds.; Academic Press: New York, 1982.
(43) Meyn, M.; Lagaly, G. *Inorg. Chem.* **1993**, *32*, 1209.
(44) Cao, G.; Mallouk, T. E. *Inorg. Chem.* **1991**, *30*, 1434.
(45) Beneke, K.; Lagaly, G. *Inorg. Chem.* **1983**, *22*, 1503.
(46) Weiss, A.; Ruthardt, R. *Z. Naturforsch.* **1973**, *28* (b), 249.
(47) Schöllhorn, R.; Sick, E.; Weiss, A. *Z. Naturforsch.* **1973**, *28* (b), 168.
(48) Lagaly, G.; Beneke, K.; Dietz, P.; Weiss, A. *Angew. Chem., Int. Ed. Engl.* **1974**, *13*, 819.
(49) Lagaly, G. *Colloid Interface Sci.* **1979**, *11*, 105.
(50) Weiss, A.; Choy, J. H. *Z. Naturforsch.* **1984**, *39* (b), 1193.

scrolling of molybdenum oxide layers. (iii) Finally, the work presented in this article yielded gram quantities of anisotropic and isotropic nanostructures utilizing cheap reactants and simple experimental procedures under ambient conditions, thus saving the efforts at harsh temperatures and high pressures.

**Supporting Information Available:** XRD patterns of $MoO_3$−NA with and without PA and the $MoO_3$−NA composite with different $MoO_3$/amine ratios and TEM images of molybdenum oxide amine composites (PDF). This material is available free of charge via the Internet at http://pubs.acs.org.

CM051685A